Stimulation of the CLIP-170–dependent capture of membrane organelles by microtubules through fine tuning of microtubule assembly dynamics

Alexis J. Lomakin[a,*,†], Pavel Kraikivski[a,*], Irina Semenova[a], Kazuho Ikeda[a], Ilya Zaliapin[b], Jennifer S. Tirnauer[c], Anna Akhmanova[d], and Vladimir Rodionov[a]

[a]R. D. Berlin Center for Cell Analysis and Modeling and Department of Cell Biology, University of Connecticut Health Center, Farmington, CT 06030; [b]Department of Mathematics and Statistics, University of Nevada–Reno, Reno, NV 89557; [c]Center for Molecular Medicine and Neag Comprehensive Cancer Center, University of Connecticut Health Center, Farmington, CT 06030; [d]Cell Biology, Faculty of Science, Utrecht University, 3584 CH Utrecht, Netherlands

ABSTRACT **Cytoplasmic microtubules (MTs) continuously grow and shorten at their free plus ends, a behavior that allows them to capture membrane organelles destined for MT minus end–directed transport. In *Xenopus* melanophores, the capture of pigment granules (melanosomes) involves the +TIP CLIP-170, which is enriched at growing MT plus ends. Here we used *Xenopus* melanophores to test whether signals that stimulate minus end MT transport also enhance CLIP-170–dependent binding of melanosomes to MT tips. We found that these signals significantly (>twofold) increased the number of growing MT plus ends and their density at the cell periphery, thereby enhancing the likelihood of interaction with dispersed melanosomes. Computational simulations showed that local and global increases in the density of CLIP-170–decorated MT plus ends could reduce the half-time of melanosome aggregation by ~50%. We conclude that pigment granule aggregation signals in melanophores stimulate MT minus end–directed transport by the increasing number of growing MT plus ends decorated with CLIP-170 and redistributing these ends to more efficiently capture melanosomes throughout the cytoplasm.**

Monitoring Editor
Alexander Mogilner
University of California, Davis

Received: Mar 28, 2011
Revised: Jul 29, 2011
Accepted: Aug 24, 2011

INTRODUCTION

Cytoplasmic microtubules (MTs) play essential roles in cell division, locomotion, spatial organization of the cytoplasm, and intracellular transport (Lane and Allan, 1998; Wittmann and Waterman-Storer, 2001; Welte, 2004; Li and Gundersen, 2008; Walczak and Heald, 2008). MTs are often organized into a polarized radial array with their minus ends clustered at the centrosome and their plus ends extended toward the cell periphery. MT plus ends continuously alternate between growing and shortening, a behavior known as dynamic instability (Mitchison and Kirschner, 1984). This dynamic behavior allows MTs to search the cytoplasm and make contacts with various intracellular targets (Kirschner and Mitchison, 1986). Among these targets are membrane organelles and cytoplasmic particles destined for movement to the cell center by means of the minus end–directed MT motor cytoplasmic dynein.

The binding of dynein cargoes to MTs is mediated by +TIPs, a group of proteins highly enriched at growing MT plus ends (Carvalho *et al.*, 2003; Galjart, 2005; Morrison, 2007; Akhmanova and Steinmetz, 2008; Gouveia and Akhmanova, 2010). In interphase cells, +TIPs are involved in the binding of membrane organelles such as endoplasmic reticulum–Golgi transport vesicles and melanosomes to MTs (Vaughan *et al.*, 2002; Lomakin *et al.*, 2009). Attachment of membrane organelles to MTs via +TIPs presumably stimulates MT minus end–directed transport because it brings dynein on the organelle surface in close proximity to the MT wall (Lomakin *et al.*, 2009). The +TIP-dependent binding of dynein cargos to MTs is likely

This article was published online ahead of print in MBoC in Press (http://www.molbiolcell.org/cgi/doi/10.1091/mbc.E11-03-0260) on August 31, 2011.

*These authors contributed equally to this work.

†Present address: Department of Cell Biology, Harvard Medical School, Boston, MA 02115.

Address correspondence to: Vladimir Rodionov (rodionov@nso.uchc.edu).

Abbreviations used: MSH, melanocyte-stimulating hormone; MTs, microtubules; PKA, protein kinase A; γTURC, γ–tubulin ring complex.

to be regulated, but the mechanisms of such regulation remain a mystery.

In this study, we used *Xenopus* melanophores to examine whether intracellular signals that induce MT minus end transport also stimulate the binding of membrane organelles to MT tips. In melanophores, thousands of membrane-bounded melanosomes (pigment granules) accumulate in the cell center (aggregation) or uniformly distribute throughout the cytoplasm (dispersion) in response to intracellular signals (Nascimento *et al.*, 2003; Kashina and Rodionov, 2005; Aspengren *et al.*, 2009). Redistribution of pigment granules is regulated by the cytoplasmic levels of cAMP and activity of the protein Kinase A (PKA; high during dispersion, low during aggregation) (Nascimento *et al.*, 2003; Kashina and Rodionov, 2005; Aspengren *et al.*, 2009). Aggregation involves the transfer of pigment granules from actin filaments to MTs, followed by transport along these MTs toward the cell center. This transfer involves capture of pigment granules by growing MT tips. Our previous work showed that CLIP-170 is the +TIP responsible for melanosome capture in the *Xenopus* melanophore system (Lomakin *et al.*, 2009). On the basis of single-microtubule imaging and computational modeling, we demonstrated that CLIP-170 is required for melanosome capture and links melanosomes to MT tips (Lomakin *et al.*, 2009). Here we sought to investigate whether pigment granule aggregation signals also enhance the number of capture events or the efficiency of the capture process.

One plausible mechanism for the regulation of melanosome binding to MTs involves reversible accumulation of CLIP-170 at MT plus ends. CLIP-170 binding to MTs is regulated by reversible phosphorylation, with phosphorylation detaching it and dephosphorylation promoting its binding to microtubules (Lee *et al.*, 2010). In support of this mechanism, phosphorylation by PKA, the major intracellular regulator of pigment granule dispersion, has been shown to reduce the binding of CLIP-170 to MTs (Lee *et al.*, 2010). Therefore, a decrease in PKA activity during pigment granule aggregation should lead to CLIP-170 dephosphorylation and accumulation at MT plus ends that could enhance the binding of melanosomes to MTs. To test this mechanism of MT minus-end transport stimulation, we compared the average length and fluorescence intensity of CLIP-170–labeled MT segments (CLIP-170 comets) in cells stimulated to aggregate or disperse melanosomes. Contrary to our expectations, we found that pigment granule aggregation signals did not significantly increase the number or distribution of CLIP-170 comets. However, we unexpectedly found that stimulation of pigment granule aggregation dramatically increased the number of growing MT tips and led to their more uniform distribution throughout the cell, thus increasing their density at the cell periphery and enhancing their overall probability of binding melanosomes. Computer simulations of pigment granule aggregation indicated that these changes would be likely to increase the rate of pigment granule aggregation significantly. We conclude that pigment granule aggregation signals stimulate the CLIP-170–dependent capture of melanosomes by inducing global changes in the spatial distribution and density of growing MT tips.

RESULTS

Pigment granule aggregation signals do not stimulate accumulation of CLIP-170 at MT tips

Our previous work showed that the initiation of MT minus end–directed movement of melanosomes during pigment granule aggregation in *Xenopus* melanophores involves their capture by growing MTs and that CLIP-170 bound to MT plus ends plays a key role in this process (Lomakin *et al.*, 2009). To determine whether pigment granule aggregation signals stimulated the capture of melanosomes by increasing the amount of CLIP-170 bound to MT plus ends, we immunostained melanophores with a CLIP-170 antibody and generated profiles of CLIP-170 fluorescence in cells stimulated to aggregate or disperse melanosomes. Quantitative analysis of the fluorescence profiles showed that the total CLIP-170 fluorescence per MT plus end was similar between cells with aggregated and dispersed pigment granules (1.04 ± 0.03 and 0.98 ± 0.03 arbitrary grayscale units, respectively). The average length of the MT tip region decorated with CLIP-170, which we determined from single-exponential fits of the decaying parts of averaged CLIP-170 profiles normalized by maximum brightness, were also similar (0.76 ± 0.07 and 0.74 ± 0.04 μm for cells stimulated to aggregate or disperse pigment granules, respectively; Figure 1). We conclude that pigment granule aggregation signals do not stimulate the capture of melanosomes by increasing the amount of CLIP-170 bound to MT plus ends or the average length of CLIP-170 comets.

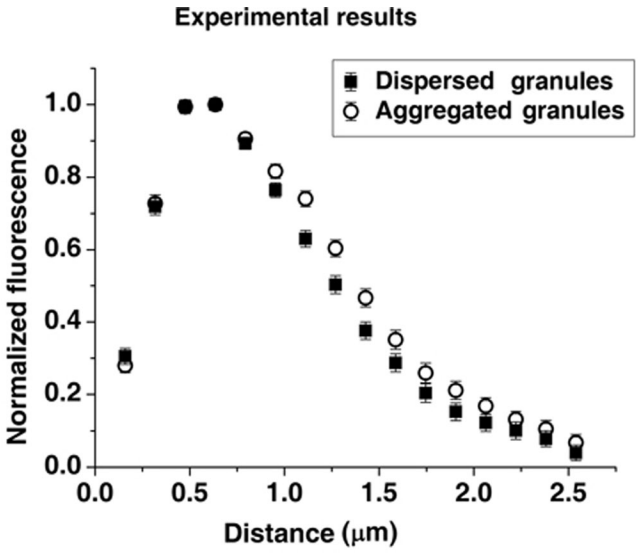

FIGURE 1: Lengths of MT segments decorated with CLIP-170 are similar between cells stimulated to aggregate or disperse pigment granules. Profiles of CLIP-170 fluorescence at MT tips normalized by maximum fluorescence and averaged for cells stimulated to aggregate (open circles) or disperse (filled squares) melanosomes. Stimulation of pigment granule aggregation does not significantly change the length of MT segments decorated by CLIP-170.

Signals that induce pigment granule aggregation increase the number of growing MT tips in the cytoplasm

An alternative mechanism for increasing melanosome capture could entail an increase in the number of growing MT plus ends decorated with CLIP-170. To test whether melanosome aggregation signals increased the number of growing MT plus ends available to capture pigment granules, we stimulated cells to aggregate or disperse pigment granules and immunostained them with antibody against the +TIP EB1. Similar to CLIP-170, EB1 has been demonstrated to bind exclusively to tips of the growing MTs (Gouveia and Akhmanova, 2010), but the EB1 antibody we used produced significantly brighter fluorescence signal than antibodies to CLIP-170 available to us, which allowed for more reliable identification of MT tips. *Xenopus* melanophores are remarkably flat cells, and all MT tips generally

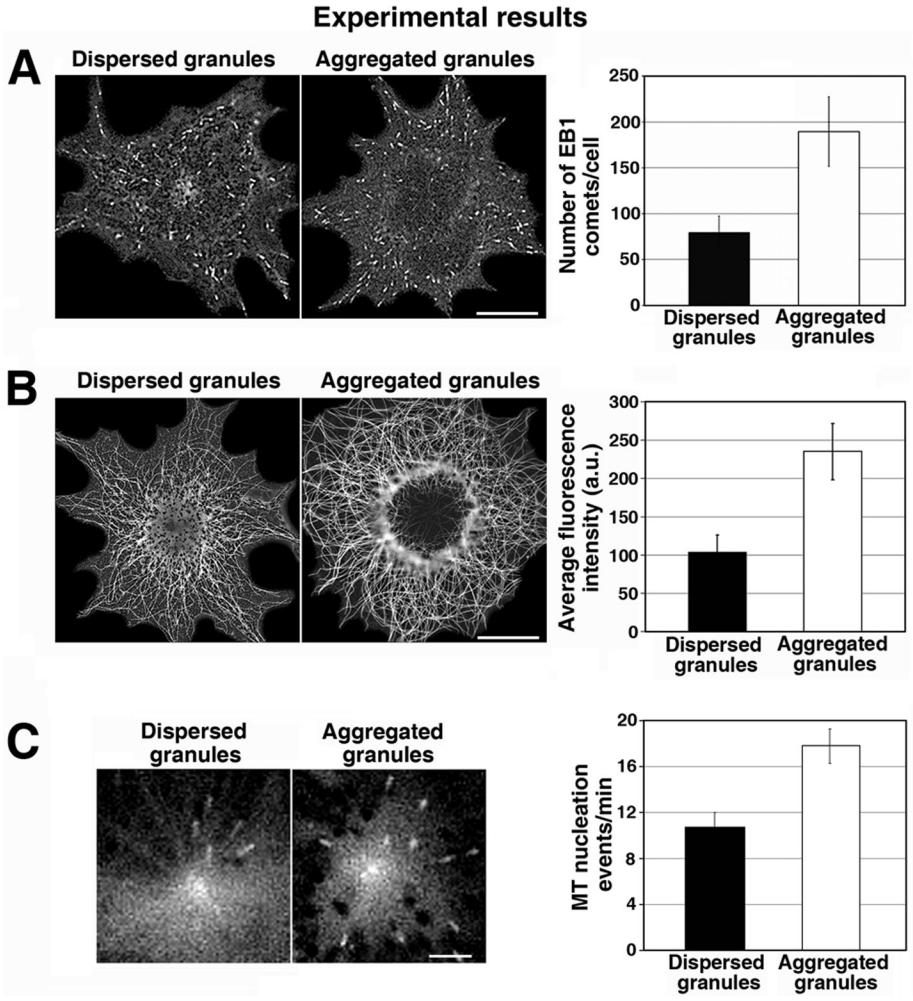

FIGURE 2: Pigment granule aggregation signals increase the total number of growing MT plus ends by stimulating MT nucleation at the centrosome. (A) Immunostaining of melanophores with an antibody against EB1. Left, images of immunostained cells; right, quantification of the average number of MT segments immunostained with EB1 antibody per cell. In melanophores with aggregated melanosomes the number of EB1-labeled segments is significantly higher than in cells with dispersed melanosomes. (B) Immunostaining of methanol-extracted-fixed melanophores with an anti-tubulin antibody. Left, images of immunostained cells; right, quantification of MT fluorescence. MT fluorescence and therefore MT polymer level are substantially higher in cells with aggregated than in those with dispersed melanosomes. (C) Measurement of the frequency of MT nucleation at the centrosome using EB1-GFP. Left, live fluorescence images of EB1-GFP at the centrosome region; right, quantification of the average number of EB1-GFP comets that emerged from the centrosome region per minute. The frequency of EB1-GFP comets that emerged from the centrosome region is higher in cells with aggregated than dispersed melanosomes.

remain in the same focal plane, which reduces the probability of detection errors. The results of immunostaining indicated that the number of growing MT plus ends was significantly higher (>twofold) in melanophores with aggregated melanosomes than in melanophores with dispersed melanosomes (Figure 2A). Total MT polymer level, quantified by measuring the fluorescence of MTs immunostained with a tubulin antibody, was also elevated, as would be expected from the stimulation of MT assembly (Figure 2B). Thus the results of these experiments indicated that pigment granule aggregation signals significantly increased the number of growing MT plus ends by enhancing MT assembly.

In melanophores, the assembly of new MTs involves their nucleation at the centrosome, followed by their polymerization. To examine whether melanosome aggregation signals enhanced MT assembly through the stimulation of MT nucleation, we quantified the rate of centrosomal MT nucleation by expressing EB1-green fluorescent protein (GFP) in melanophores and counting the number of EB1-labeled comets emerging from the centrosome region over time. We found that the number of GFP-EB1 comets emerging from the centrosome area per unit time was 1.6 times higher in melanophores with aggregated than in those with dispersed melanosomes (Figure 2C). We conclude that pigment granule aggregation signals enhance MT nucleation at the centrosome and therefore increase the number of growing MT tips available for the binding of pigment granules.

The density of growing MT tips at the cell periphery is higher in cells with aggregated than in cells with dispersed melanosomes

Another parameter that could affect the probability of pigment granule capture by growing MT plus ends is the distribution of these plus ends within the cytoplasm. Because pigment granules are initially dispersed throughout the cytoplasm, a more even distribution of growing MT tips, increasing their density at the cell periphery, would be expected to enhance granule capture events. To determine whether pigment granule aggregation signals induced the accumulation of growing MT plus ends at the cell periphery, we stimulated cells to aggregate or disperse melanosomes and generated plots of EB1 comet density as a function of distance from the cell center by counting comet density in each of five areas delineated by concentric circles equidistantly distributed along the cell radius (Figure 3A). We found that in cells induced to disperse melanosomes, the EB1 comet density was more than fivefold less at the cell margins than at the cell center, whereas in melanophores stimulated to aggregate pigment granules, the density distribution was close to uniform throughout the cytoplasm (Figure 3B, closed circles and squares, respectively). This result indicated that pigment granule aggregation signals increased the density of growing MT plus ends at the cell periphery, resulting in an array of capture-competent MT plus ends that covered the entire cytoplasmic space.

Our finding of an increased number of growing MT tips at the cell periphery in cells stimulated to aggregate pigment granules suggested that the average MT length was greater in these cells. Average MT length is determined by the relative contributions of plus end growth and shortening, which are in turn defined by the parameters of MT dynamic instability—durations of growth and shortening events, growth and shortening rates, frequencies of transitions from growth to shortening (catastrophe) and from shortening

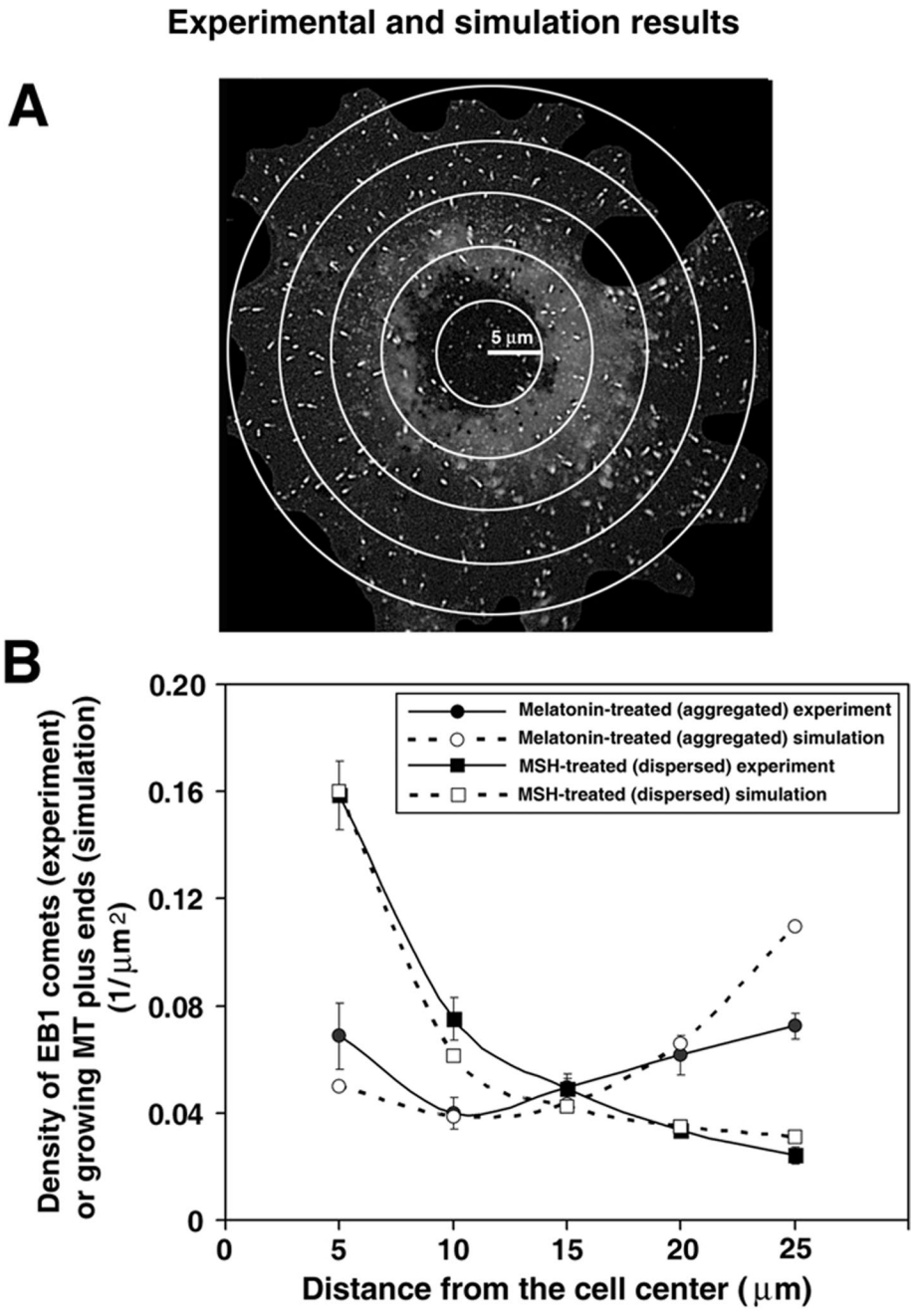

FIGURE 3: Pigment granule aggregation stimuli increase the density of growing MT plus ends at the cell periphery by changing the parameters of MT dynamic instability. (A) Method for the measurement of density distribution of growing MT plus ends along the cell radius. EB1 comets were counted within each of five regions delineated with concentric circles placed at the same distance from each other over fluorescence images of immunostained cells. (B) EB1 comet counts were normalized for each region area, and data obtained for cells treated to aggregate (circles) or disperse (squares) melanosomes were averaged and used to generate plots of EB1 comet density as a function of distance along the cell radius. Closed symbols represent experimental data. Open symbols show the values determined by computer simulations of MT dynamics based on parameters of MT dynamic instability. Error bars represent SE of the mean. Computational and experimental data agree with each other and show that in melanophores with dispersed melanosomes the density of growing MT plus ends decreases with increasing distance from the cell center, whereas in cells stimulated to aggregate pigment granules, growing MT plus end density is approximately similar at the cell center and the cell periphery.

to growth (rescue), and lengths of periods of apparent absence of growth or shortening (pauses). To determine whether pigment granule aggregation signals changed these parameters in a way that increased the average length of MTs, we tracked MT tips in cells with fluorescently labeled MTs and decomposed the tip trajectories into the phases of growth and shortening using the Multiscale Trend Analysis algorithm that we developed (Zaliapin *et al.*, 2004). Remarkably, we found that pigment granule aggregation signals changed all of the major parameters of MT dynamic instability. Durations and rates of MT growth and shortening events decreased by ~50 and ~30%, respectively, whereas rescue and catastrophe frequencies increased (Table 1). Significantly, in cells with dispersed melanosomes, the net growth and shortening of MTs (calculated by multiplying average distances of growth or shortening events by the fractions of time MTs spent growing or shortening, respectively) were balanced (3.43 and 3.28 μm, respectively), whereas in cells with aggregated pigment granules, the net MT growth distance (1.56 μm) significantly exceeded the net shortening distance (0.66 μm). Thus pigment granule aggregation signals increased the local density of growing MT plus ends in the peripheral regions of the cell by inducing changes in MT plus-end dynamics that increased the average MT length.

To confirm that MT dynamic instability parameters measured in melanophores with aggregated melanosomes could account for the accumulation of MT plus ends at the cell periphery, we used a two-dimensional computational model for MT dynamics that allowed us to calculate the steady-state density distribution of growing MT plus ends as a function of distance from the cell center based on parameters of MT dynamic instability (Lomakin *et al.*, 2009). In the model, we assumed that each melanophore had a circular shape with a radius of 27 μm and contained a radial array of MTs undergoing dynamic instability at plus ends with parameters experimentally measured for each signaling state (Table 1). The average number of MTs in the array was determined by estimating the average number of EB1 comets per cell and normalizing to the total time MTs spent in all phases of the growth and shortening cycle. This resulted in 370 MTs for cells with aggregated and 160 for cells with dispersed melanosomes (Supplemental Table S1). We assumed that MTs that reached the cell margin stopped growing and began shortening immediately. Testing alternative boundary condition behaviors convinced us that this assumption was valid (Supplemental Text). Microtubules that completely disassembled were replaced by the immediate nucleation of a new MT at the centrosome, thus keeping the total number of MTs at a constant level.

	Dispersed pigment	Aggregated pigment	Dispersed pigment + H89
Growth distance (μm)	6.13 ± 0.46	2.59 ± 0.09	2.50 ± 0.10
Growth rate (μm/s)	0.23 ± 0.03	0.16 ± 0.01	0.18 ± 0.01
Shortening distance (μm)	7.72 ± 0.66	2.06 ± 0.08	2.51 ± 0.09
Shortening rate (μm/s)	0.25 ± 0.01	0.18 ± 0.01	0.21 ± 0.01
Catastrophe frequency (s^{-1})	0.016 ± 0.002	0.026 ± 0.002	0.030 ± 0.002
Rescue frequency (s^{-1})	0.019 ± 0.001	0.033 ± 0.001	0.033 ± 0.002
Pause duration (s)	3.45 ± 0.17	4.42 ± 0.19	4.08 ± 0.21
Number of analyzed MTs	60	40	30
Number of analyzed cells	13	8	8

TABLE 1: Parameters of MT dynamic instability in melanophores stimulated to aggregate or disperse pigment granules or treated with the PKA inhibitor H89.

On the basis of these parameters, we computed the distribution of growing MT ends, and these computational data matched remarkably well with the experimentally measured distribution of EB1 comet density (Figure 3B). In cells with dispersed melanosomes, both experimentally measured and computed distributions of growing MT plus ends gradually dropped at the cell periphery, whereas in melanophores with aggregated pigment granules their density was more uniformly distributed both in experimental observation and the computational model (Figure 3B). The only significant difference between the experimental and computational results was observed at the cell margin in melanophores with aggregated pigment granules. Namely, the computational data showed a higher MT density than we observed experimentally. This difference was likely explained by an underestimation of EB1 comet density at the cell borders from the experimental images (Figure 3B). Thus our computer simulations closely matched our experimental measurements. We conclude that pigment granule aggregation signals changed the parameters of MT dynamic instability in a manner that produced net MT growth, thus increasing the local density of growing MT plus ends at the cell periphery.

Local and global changes in the density of CLIP-170–labeled MT plus ends significantly accelerate the aggregation of pigment granules

The results of our experiments showed that pigment granule aggregation signals changed MT nucleation and polymerization dynamics, which increased the global density of CLIP-170–labeled MT plus ends and their distribution in the cell. These global changes in the density of MT plus ends decorated with CLIP-170 were expected to facilitate the capture of melanosomes by MTs and therefore to account for an increase in pigment granule aggregation. However, the extent of this acceleration was impossible to estimate experimentally because we could not isolate changes in melanosome movement from MT dynamics changes. Therefore, to determine the sole effect of the increase in growing CLIP-170–labeled MT plus ends, we used this same computational model to which we added a new parameter that incorporated the capture of pigment granules by growing MT tips and the movement of these granules to the cell center along MTs (Lomakin *et al.*, 2009). The expanded model computed the kinetics of granule aggregation based on the parameters of MT dynamics, the probability of pigment granule capture, and the bidirectional movement of captured melanosomes to the cell center and generated a parameter called gray level decrease, which predicts how fast the dark peripheral cytoplasm becomes transparent due to granule aggregation (Figure 4, top; see the

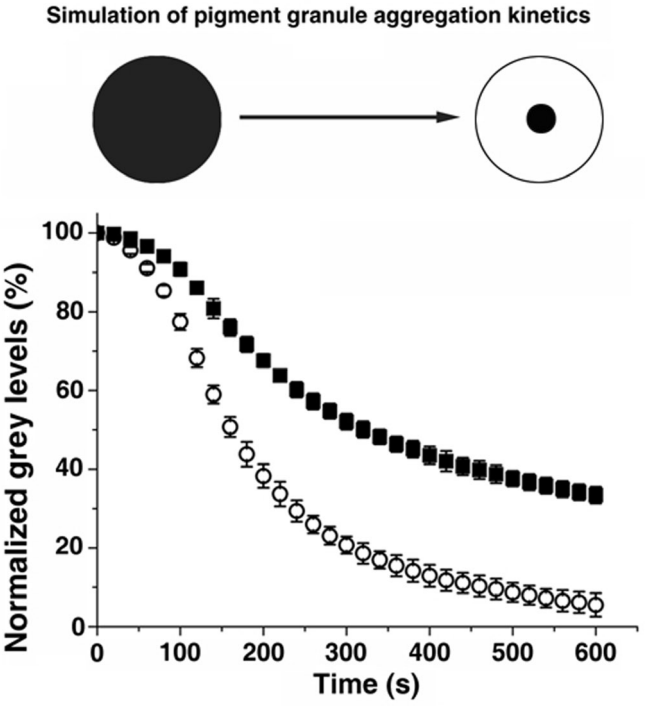

FIGURE 4: Changes in MT dynamic instability and nucleation induced by pigment granule aggregation stimuli significantly increase the rate of pigment granule aggregation. Top, cartoon illustrating the principle of the method used for computing the kinetics of pigment granule aggregation. In the dispersed state, a homogeneous pigment granule distribution makes the cytoplasm dark. In this state, gray level (the measure of darkness of the cytoplasm) is designated to be 100%. During aggregation, the cytoplasm becomes increasingly transparent, and gray level drops to a fraction of the initial value. Bottom, comparison of pigment granule aggregation kinetics. Open circles represent the gray level kinetics in a virtual melanophore with the granule movement and MT parameters associated with aggregation; black squares represent the gray level kinetics in a virtual melanophore with the granule movement parameters associated with aggregation and the MT parameters associated with dispersion. Data are expressed as the gray level percentage change with time. The error bars reflect the mean square displacement over at least 10 simulations per parameter set. Microtubule parameters associated with aggregation result in a significantly faster gray level decrease.

Supplemental Text of Lomakin *et al*. [2009] for a full description of the model and Supplemental Table 1 for a complete list of the current model parameters).

In this expanded model, we included several assumptions. We assumed that in the dispersed state melanosomes were undergoing a random walk along actin filaments, which was defined by the effective diffusion coefficient (Semenova *et al*., 2008). Capture by a polymerizing microtubule end was assumed to have occurred if the distance between the center of a moving melanosome and the distal segment of a growing MT decorated with CLIP-170 became less than or equal to the melanosome radius (0.25 μm). We assumed that 74.9 ± 15.7% of the capture events resulted in initiation of melanosome movement along MTs, based on our published observations (Lomakin et al. 2009). On a rare occasion when the rate of MT shortening exceeded the velocity of minus end–directed granule movement, we assumed that the melanosome would detach from the MT and resume actin-dependent transport. Our previous analysis showed that this model faithfully reproduced the kinetics of pigment granule aggregation (Lomakin *et al*., 2009).

We next used this expanded model to determine how the changes in the distribution and density of MT plus ends described earlier increased the rate of granule aggregation.

We simulated pigment granule aggregation in a virtual melanophore to which we assigned the granule movement parameters measured in cells undergoing melanosome aggregation and combined these with the MT number and dynamics parameters from cells undergoing dispersion. The results of these simulations showed that MT parameters had a major effect on granule aggregation. Specifically, the kinetics of gray level decrease was slowed significantly, as evidenced from kinetic curves (Figure 4, bottom). The calculated half-times of gray level decrease were 162.9 ± 7.5 s for MT parameters associated with aggregation and 322.3 ± 15.5 s for parameters associated with dispersion, an ~50% decrease. We conclude that changes in MT assembly dynamics that we observed upon stimulation of pigment granule aggregation could significantly accelerate pigment granule aggregation.

Changes in centrosomal MT nucleation and dynamic instability at plus ends are mediated by PKA

Our data showed that pigment granule aggregation signals modified centrosomal MT nucleation and MT dynamics, which in turn stimulated the capture of pigment granules by CLIP-170–labeled MT tips and increased the rate of melanosome aggregation. In *Xenopus* melanophores, the direction of pigment granule transport is regulated by the level of the second messenger cAMP, which is high during dispersion and low during aggregation. High cAMP levels increase the activity of PKA, which controls pigment granule–bound MT motors (Kashina *et al*., 2004). To test the possibility that PKA also regulated the microtubule parameters studied here, we measured the rate of MT nucleation at the centrosome, parameters of MT dynamic instability, and distribution of growing MT plus ends in melanophores with dispersed pigment granules treated with the cell-permeable PKA inhibitor H89. We found that treatment of melanophores with H89 increased the frequency of centrosomal MT nucleation from 10.3 ± 1.3/min in cells stimulated with melanocyte-stimulating hormone (MSH; dispersion signal) to 16.3 ± 1.9/min in cells stimulated with MSH and treated with H89. This nucleation frequency in the presence of H89 was similar to the frequency determined for melatonin (aggregation signal)-treated cells with aggregated pigment granules (17.0 ± 1.5/min). We also found that H89 treatment induced changes in parameters of MT dynamic instability analogous to those observed after stimulation of pigment granule aggregation with melatonin (Table 1). Finally, we discovered that the distribution of growing MT plus ends in H89-treated cells matched the distribution observed in cells with aggregated pigment granules and was significantly different from the distribution determined for melanophores with dispersed melanosomes (Supplemental Figure S6). We conclude that changes in MT assembly dynamics observed upon stimulation of pigment granule aggregation were caused by a decrease in PKA activity.

DISCUSSION

Stimulation of pigment granule capture by MTs

In this article, we show that intracellular signals that activate MT minus end–directed transport in melanophores (aggregation signals) also enhance the capture of membrane-bound pigment granules by growing MT tips. Several lines of evidence indicate that these aggregation signals increase the likelihood of interaction between pigment granules and MTs. First, aggregation signals promote the nucleation of new MTs and therefore substantially increase the total number of growing MT plus ends available for binding pigment granules. Second, these signals induce changes in the parameters of MT plus end dynamic instability such that their net growth increases, leading to a redistribution of growing MT tips throughout the cytoplasm to better match the distribution of granules. Finally, the results of computer simulations demonstrate that these changes in the number and distribution of growing MT plus ends could account for a major increase in the rate of pigment granule aggregation. Therefore our work for the first time demonstrates that changes in MT nucleation and dynamics can regulate the capture of membrane organelles in interphase cells.

Molecular mechanisms that regulate the binding of melanosomes to MT tips are poorly understood. Our data indicate that aggregation signals do not enhance pigment granule binding by increasing the accumulation of CLIP-170 at MT plus ends. This lack of stimulation of CLIP-170 accumulation was surprising, given that the binding of CLIP-170 to MTs is known to be inhibited by phosphorylation with PKA (Lee *et al*., 2010), the activity of which sharply drops during pigment granule aggregation (Nascimento *et al*., 2003; Aspengren *et al*., 2009). However, the results of our experiments do not exclude additional regulatory mechanisms based on the affinity of pigment granules for MTs. CLIP-170 is a prototypic +TIP that was shown to mediate the binding of organelles to MTs (Rickard and Kreis, 1996; Perez *et al*., 1999). Our past work suggests that CLIP-170 associates with melanosomes through an adaptor protein on their surface, and it is possible that melanosome aggregation signals stimulate the binding of CLIP-170 to such a putative adaptor protein (Lomakin *et al*., 2009). Thus, in addition to increasing the probability of melanosome capture events, pigment granule aggregation signals might also enhance the efficiency of these capture events.

Regulation of MT nucleation at the centrosome

Our data show for the first time that pigment granule aggregation signals induce a dramatic increase in the total number of MTs in the cytoplasm of melanophores and indicate that this increase is associated with nucleation of new MTs at the centrosome. Furthermore, our results also show that this stimulation of centrosomal MT nucleation is induced by a drop in activity of the PKA. We envision two hypothetical mechanisms for the negative regulation of centrosomal MT nucleation by PKA.

The first mechanism involves regulation of γ-tubulin ring complexes (γTuRCs) that provide nucleation templates for MT growth at the centrosome (Zheng *et al*., 1998). We suggest that this regulation

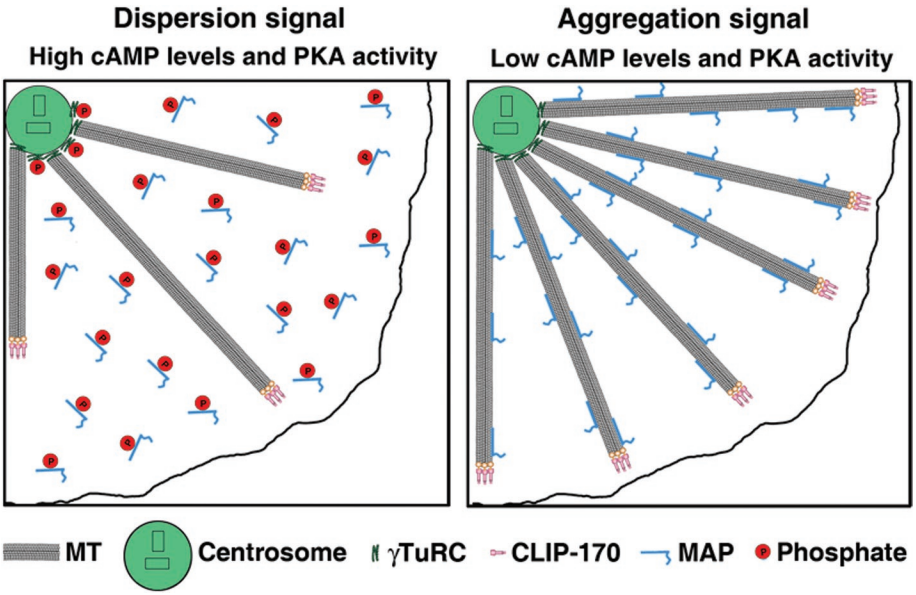

FIGURE 5: Model for MT regulation in melanophores. Left, in cells stimulated to disperse pigment granules, cAMP levels and the activity of PKA are high, which leads to phosphorylation and inactivation of centrosomal proteins involved in MT nucleation, such as γTuRC, and cytoplasmic microtubule-associated proteins responsible for MT polymerization, which reduces the number of growing MT plus ends and decreases their density at the cell periphery. Right, pigment granule aggregation signals decrease cAMP levels and PKA activity, which relieves the PKA-dependent inhibition of MT nucleation and growth. As a result, more MTs nucleate at the centrosome and persistently grow to the cell periphery, thus increasing the total number and local density of MT ends at the cell periphery. Increases in the local density of growing MT plus ends at the cell periphery and their total number throughout the cytoplasm enhance pigment granule aggregation.

implicates the PKA pool associated with the centrosome, which controls recruitment of γTuRCs to the centrosome, or the MT-nucleating activity of γTuRCs already bound to the centrosome. At high cAMP levels typical for melanophores with dispersed melanosomes, active PKA scaffolded at the centrosome by A-kinase adaptor proteins phosphorylates centrosomal proteins, and this phosphorylation directly or indirectly inhibits γTuRC recruitment or activation (Takahashi *et al.*, 1999; Witczak *et al.*, 1999; Flory *et al.*, 2000; Li *et al.*, 2001). A drop in cAMP levels during melanosome aggregation inhibits PKA activity and leads to dephosphorylation of PKA substrates by centrosome-associated protein phosphatases (Huang *et al.*, 2005; Flegg *et al.*, 2010). Dephosphorylation relieves the inhibitory effect of PKA on MT nucleation by enhancing recruitment or activation of γTuRC, which stimulates MT nucleation and therefore increases the number of MTs growing from the centrosomal region.

The second mechanism includes regulation of MT assembly by PKA on a cell-wide scale through changes in the activities of soluble proteins not associated directly with the centrosome. Studies of MT nucleation on isolated centrosomes in vitro indicate that stimulation of MT assembly allows more growth from the centrosome because it engages additional weak MT nucleation sites (Meda *et al.*, 1997; Andersen, 1999). Stimulation of MT assembly might also promote MT nucleation on the surface of pigment granules, which have been shown to nucleate MTs in cytoplasmic fragments of melanophores lacking centrosomes (Vorobjev *et al.*, 2001). If pigment granules nucleate MTs in intact cells, then their accumulation in the cell center should generate more MTs, whose growth to the cell periphery would further amplify the size of the MT array and provide further sites for the capture of trailing melanosomes, increasing the rate of pigment granule aggregation.

Regulation of MT dynamics

The results of our experiments indicate that pigment granule aggregation signals induce the accumulation of growing MT tips throughout the cell and that this accumulation is explained by changes in the parameters of MT dynamic instability at MT plus ends. Our data indicate that, in contrast to melanophores induced to disperse pigment granules, in cells stimulated to aggregate melanosomes the average growth distance exceeds the average shortening distance, and the rescue frequency is higher than the catastrophe frequency. We hypothesize that modification of MT dynamic instability parameters involves the activation of protein factors, such as MAP4 (Chapin and Bulinski, 1991), XMAP215 (Gard and Kirschner, 1987; Kinoshita *et al.*, 2002), or EB1 (Komarova *et al.*, 2009), which promote MT assembly (Holmfeldt *et al.*, 2009; van der Vaart *et al.*, 2009). Remarkably, in cells stimulated to aggregate pigment granules, the catastrophe frequency also increases, which allows MTs to remain highly dynamic and continue to capture melanosomes. Thus melanosome aggregation signals might simultaneously stimulate activities of MT assembly–promoting factors and proteins that induce MT catastrophes, such as Op18/stathmin (Belmont and Mitchison, 1996; Cassimeris, 2002), and/or XKCM1 (Walczak *et al.*, 1996; Kinoshita *et al.*, 2006). Furthermore, to maintain the steady-state levels of tubulin subunits in the cytoplasm, the net growth of MTs at the plus ends should be compensated by minus end shortening, which could involve release of MTs from the centrosome. Therefore MT-severing enzymes, such as katanin (McNally and Vale, 1993; Roll-Mecak and McNally, 2010), could also be activated by pigment granule aggregation signals. Thus stimulation of pigment granule aggregation apparently induces concerted changes in the activities of protein factors that regulate all major aspects of MT dynamics and assembly.

A model for regulation of MTs during pigment granule aggregation

On the basis of our results, we propose a model for changes in MT nucleation and dynamics induced by melanosome aggregation signals (Figure 5). We suggest that at high cAMP levels characteristic for cells with dispersed melanosomes, PKA is active, and PKA-dependent phosphorylation inactivates proteins involved in centrosomal MT nucleation and MT polymerization dynamics, thus decreasing MT polymer levels and the number of growing MT plus ends available for capturing pigment granules. Pigment granule aggregation signals reduce cAMP levels and PKA activity and result in the dephosphorylation and activation of MT nucleation– and assembly–promoting proteins, leading to the stimulation of MT assembly at the centrosome and the persistent growth of MTs toward the cell periphery. Global increases in the number of CLIP-170–decorated MT plus ends and local increases in their density in outer regions of the cell enhance the probability of pigment granule capture and therefore accelerate pigment granule aggregation. Testing changes in activities of PKA substrates affecting MT nucleation and assembly

predicted by our model is an exciting new direction for future research.

MATERIALS AND METHODS

Cell culture and H89 treatment

Xenopus melanophores (Kashina *et al*., 2004) were cultured in 70% L15 medium supplemented with antibiotics, 20% fetal bovine serum, and 5 μg/ml insulin at 27°C. Prior to stimulation of aggregation or dispersion, cells were transferred into serum-free 70% L15 medium and incubated for at least 1 h at 27°C. Aggregation of melanosomes was induced with 10^{-8} M melatonin. For dispersion of melanosomes, cells were treated with 10^{-8} M MSH. These treatments did not alter the size or shape of melanophores.

To inhibit PKA activity, melanophores were incubated for 15 min at room temperature in the presence of the PKA inhibitor H89 (30 μM).

DNA constructs and transfection

EB1-GFP was described by Stepanova *et al*. (2003). Cells were transfected using Lipofectamine 2000 (Invitrogen, Carlsbad, CA) according to manufacturer's instructions and incubated for 1–2 d at 27°C for protein expression.

Microinjection

Conjugation of porcine brain tubulin with Cy3 and pressure microinjection of melanophores with Cy3-tubulin (6–7 mg/ml) were performed as described by Ikeda *et al.* (2010).

Immunostaining

For immunostaining with antibody against CLIP-170, cells were washed with phosphate-buffered saline (PBS), fixed in cold (−20°C) methanol for 10 min, postfixed with 4% formaldehyde for 10 min at room temperature, permeabilized with 0.1% Triton X-100, and incubated with rabbit antibody against CLIP-170 (no. 2221; Komarova *et al*., 2002) and goat anti-rabbit antibody conjugated with Alexa Fluor 488 (Invitrogen). For immunostaining with tubulin and EB1 antibodies, melanophores were washed with PBS and fixed with cold methanol. After rehydration in PBS, cells were incubated with mouse monoclonal tubulin antibody DM1A (Sigma-Aldrich, St. Louis, MO) or EB1 antibody (BD Transduction Laboratories, Franklin Lakes, NJ) and Alexa Fluor 488–labeled rabbit anti–mouse antibody (Invitrogen).

Image acquisition and analysis

Fluorescence microscopy of melanophores was performed using a Nikon TE300 inverted microscope equipped with a Plan ×100 1.25–numerical aperture objective lens. Fluorescence images were acquired with an iXon EM-CCD camera (Andor Technology, Windsor, CT) driven by Metamorph image acquisition and analysis software (Universal Imaging, Downington, PA). Live imaging of cells injected with Cy3-tubulin or transfected with EB1-GFP were performed in the presence of oxygen scavenger Oxyrase (Oxyrase Company, Mansfield, OH) to reduce photodamage (Ikeda *et al*., 2010).

MT dynamics were measured by acquiring time-series of images of Cy3-labeled MTs and manually tracking individual MT ends using Metamorph software. Parameters of MT dynamic instability were determined by decomposing the trajectories of MT ends into phases of growth or shortening and pauses using Multiscale Trend Analysis as described by Lomakin *et al*. (2009).

The frequency of MT nucleation at the centrosome was estimated from time series of images of melanophores expressing EB1-GFP (Piehl and Cassimeris, 2003; Piehl *et al*., 2004) by counting the EB1-GFP comets that emerged from the centrosome area delineated with a 12 × 12 μm box.

MT polymer levels were quantified using the method of Piehl *et al*. (2004) by measuring MT fluorescence in methanol-extracted cells immunostained with tubulin antibody. Sixteen-bit images of MTs were taken with an exposure time of 1 s, and the average pixel reading was determined using Metamorph software within a 15 × 15 μm box in three different areas of the cell lamella. Average background fluorescence was measured in regions of images outside the cell and subtracted from cell fluorescence. Fluorescence measurements were performed for 10 cells in each signaling state.

Distribution of growing MT plus ends along the cell radius was determined by counting MT segments immunostained with antibody against the +TIP EB1 (EB1 comets) in each of five regions delineated by concentric circles placed at a distance 5 μm from each other over a fluorescence image of a cell with the radius ~27 μm (Figure 3A). EB1 comet counts were normalized for each region area, and data obtained for cells treated to aggregate or disperse melanosomes or treated with PKA inhibitor H89 were averaged and plotted as a function of distance along the cell radius. Twenty cells in each experimental condition were used for analysis.

To measure the length of CLIP-170 comets and the amount of CLIP-170 bound to MT ends, melanophores treated to aggregate or disperse pigment granules were immunostained with a CLIP-170 antibody, and fluorescence images of cells were acquired at the same excitation light intensity. After background subtraction, images were used to generate profiles of CLIP-170 fluorescence intensity at MT tips with the line scan function of Metamorph. Approximately 100 fluorescence intensity profiles were obtained for cells induced to aggregate or disperse pigment granules (five each). The amount of MT-bound CLIP-170 was calculated by integrating fluorescence in every profile. For the measurement of average length of CLIP-170 comets, CLIP-170 fluorescence intensity profiles were normalized to maximum brightness and averaged separately for each signaling state. Average length of CLIP-170 comets was measured by fitting normalized averaged profiles by a single-exponential function as described by Bieling *et al.* (2007, 2008).

ACKNOWLEDGMENTS

We thank Olga Zhapparova for a critical reading of the manuscript. This work was supported by National Institutes of Health Grants GM62290 (V.I.R) and P41RR013186 (V.I.R. and P.K).

REFERENCES

Akhmanova A, Steinmetz MO (2008). Tracking the ends: a dynamic protein network controls the fate of microtubule tips. Nat Rev Mol Cell Biol 9, 309–322.

Andersen SS (1999). Molecular characteristics of the centrosome. Int Rev Cytol 187, 51–109.

Aspengren S, Hedberg D, Skold HN, Wallin M (2009). New insights into melanosome transport in vertebrate pigment cells. Int Rev Cell Mol Biol 272, 245–302.

Belmont LD, Mitchison TJ (1996). Identification of a protein that interacts with tubulin dimers and increases the catastrophe rate of microtubules. Cell 84, 623–631.

Bieling P, Kandels-Lewis S, Telley IA, van Dijk J, Janke C, Surrey T (2008). CLIP-170 tracks growing microtubule ends by dynamically recognizing composite EB1/tubulin-binding sites. J Cell Biol 183, 1223–1233.

Bieling P, Laan L, Schek H, Munteanu EL, Sandblad L, Dogterom M, Brunner D, Surrey T (2007). Reconstitution of a microtubule plus-end tracking system in vitro. Nature 450, 1100–1105.

Carvalho P, Tirnauer JS, Pellman D (2003). Surfing on microtubule ends. Trends Cell Biol 13, 229–237.

Cassimeris L (2002). The oncoprotein 18/stathmin family of microtubule destabilizers. Curr Opin Cell Biol 14, 18–24.

Chapin SJ, Bulinski JC (1991). Non-neuronal 210 × 10(3) Mr microtubule-associated protein (MAP4) contains a domain homologous to the microtubule-binding domains of neuronal MAP2 and tau. J Cell Sci 98, 27–36.
Flegg CP, Sharma M, Medina-Palazon C, Jamieson C, Galea M, Brocardo MG, Mills K, Henderson BR (2010). Nuclear export and centrosome targeting of the protein phosphatase 2A subunit B56alpha: role of B56alpha in nuclear export of the catalytic subunit. J Biol Chem 285, 18144–18154.
Flory MR, Moser MJ, Monnat RJ Jr, Davis TN (2000). Identification of a human centrosomal calmodulin-binding protein that shares homology with pericentrin. Proc Natl Acad Sci USA 97, 5919–5923.
Galjart N (2005). CLIPs and CLASPs and cellular dynamics. Nat Rev Mol Cell Biol 6, 487–498.
Gard DL, Kirschner MW (1987). A microtubule-associated protein from *Xenopus* eggs that specifically promotes assembly at the plus-end. J Cell Biol 105, 2203–2215.
Gouveia SM, Akhmanova A (2010). Cell and molecular biology of microtubule plus end tracking proteins: end binding proteins and their partners. Int Rev Cell Mol Biol 285, 1–74.
Holmfeldt P, Sellin ME, Gullberg M (2009). Predominant regulators of tubulin monomer-polymer partitioning and their implication for cell polarization. Cell Mol Life Sci 66, 3263–3276.
Huang HS, Pozarowski P, Gao Y, Darzynkiewicz Z, Lee EY (2005). Protein phosphatase-1 inhibitor-3 is co-localized to the nucleoli and centrosomes with PP1gamma1 and PP1alpha, respectively. Arch Biochem Biophys 443, 33–44.
Ikeda K, Semenova I, Zhapparova O, Rodionov V (2010). Melanophores for microtubule dynamics and motility assays. Methods Cell Biol 97, 401–414.
Kashina A, Rodionov V (2005). Intracellular organelle transport: few motors, many signals. Trends Cell Biol 15, 396–398.
Kashina AS, Semenova IV, Ivanov PA, Potekhina ES, Zaliapin I, Rodionov VI (2004). Protein kinase A, which regulates intracellular transport, forms complexes with molecular motors on organelles. Curr Biol 14, 1877–1881.
Kinoshita K, Habermann B, Hyman AA (2002). XMAP215: a key component of the dynamic microtubule cytoskeleton. Trends Cell Biol 12, 267–273.
Kinoshita K, Noetzel TL, Arnal I, Drechsel DN, Hyman AA (2006). Global and local control of microtubule destabilization promoted by a catastrophe kinesin MCAK/XKCM1. J Muscle Res Cell Motil 27, 107–114.
Kirschner M, Mitchison T (1986). Beyond self-assembly: from microtubules to morphogenesis. Cell 45, 329–342.
Komarova Y *et al.* (2009). Mammalian end binding proteins control persistent microtubule growth. J Cell Biol 184, 691–706.
Komarova YA, Akhmanova AS, Kojima S, Galjart N, Borisy GG (2002). Cytoplasmic linker proteins promote microtubule rescue in vivo. J Cell Biol 159, 589–599.
Lane J, Allan V (1998). Microtubule-based membrane movement. Biochim Biophys Acta 1376, 27–55.
Lee HS *et al.* (2010). Phosphorylation controls autoinhibition of cytoplasmic linker protein-170. Mol Biol Cell 21, 2661–2673.
Li Q, Hansen D, Killilea A, Joshi HC, Palazzo RE, Balczon R (2001). Kendrin/pericentrin-B, a centrosome protein with homology to pericentrin that complexes with PCM-1. J Cell Sci 114, 797–809.
Li R, Gundersen GG (2008). Beyond polymer polarity: how the cytoskeleton builds a polarized cell. Nat Rev Mol Cell Biol 9, 860–873.
Lomakin AJ, Semenova I, Zaliapin I, Kraikivski P, Nadezhdina E, Slepchenko BM, Akhmanova A, Rodionov V (2009). CLIP-170-dependent capture of membrane organelles by microtubules initiates minus-end directed transport. Dev Cell 17, 323–333.
McNally FJ, Vale RD (1993). Identification of katanin, an ATPase that severs and disassembles stable microtubules. Cell 75, 419–429.
Meda P, Chevrier V, Edde B, Job D (1997). Demonstration and analysis of tubulin binding sites on centrosomes. Biochemistry 36, 2550–2558.
Mitchison T, Kirschner M (1984). Dynamic instability of microtubule growth. Nature 312, 237–242.
Morrison EE (2007). Action and interactions at microtubule ends. Cell Mol Life Sci 64, 307–317.
Nascimento AA, Roland JT, Gelfand VI (2003). Pigment cells: a model for the study of organelle transport. Annu Rev Cell Dev Biol 19, 469–491.
Perez F, Diamantopoulos GS, Stalder R, Kreis TE (1999). CLIP-170 highlights growing microtubule ends in vivo. Cell 96, 517–527.
Piehl M, Cassimeris L (2003). Organization and dynamics of growing microtubule plus ends during early mitosis. Mol Biol Cell 14, 916–925.
Piehl M, Tulu US, Wadsworth P, Cassimeris L (2004). Centrosome maturation: measurement of microtubule nucleation throughout the cell cycle by using GFP-tagged EB1. Proc Natl Acad Sci USA 101, 1584–1588.
Rickard JE, Kreis TE (1996). CLIPs for organelle-microtubule interactions. Trends Cell Biol 6, 178–183.
Roll-Mecak A, McNally FJ (2010). Microtubule-severing enzymes. Curr Opin Cell Biol 22, 96–103.
Semenova I, Burakov A, Berardone N, Zaliapin I, Slepchenko B, Svitkina T, Kashina A, Rodionov V (2008). Actin dynamics is essential for myosin-based transport of membrane organelles. Curr Biol 18, 1581–1586.
Stepanova T, Slemmer J, Hoogenraad CC, Lansbergen G, Dortland B, De Zeeuw CI, Grosveld F, van Cappellen G, Akhmanova A, Galjart N (2003). Visualization of microtubule growth in cultured neurons via the use of EB3-GFP (end-binding protein 3-green fluorescent protein). J Neurosci 23, 2655–2664.
Takahashi M, Shibata H, Shimakawa M, Miyamoto M, Mukai H, Ono Y (1999). Characterization of a novel giant scaffolding protein, CG-NAP, that anchors multiple signaling enzymes to centrosome and the Golgi apparatus. J Biol Chem 274, 17267–17274.
van der Vaart B, Akhmanova A, Straube A (2009). Regulation of microtubule dynamic instability. Biochem Soc Trans 37, 1007–1013.
Vaughan PS, Miura P, Henderson M, Byrne B, Vaughan KT (2002). A role for regulated binding of p150(Glued) to microtubule plus ends in organelle transport. J Cell Biol 158, 305–319.
Vorobjev I, Malikov V, Rodionov V (2001). Self-organization of a radial microtubule array by dynein-dependent nucleation of microtubules. Proc Natl Acad Sci USA 98, 10160–10165.
Walczak CE, Heald R (2008). Mechanisms of mitotic spindle assembly and function. Int Rev Cytol 265, 111–158.
Walczak CE, Mitchison TJ, Desai A (1996). XKCM1: a *Xenopus* kinesin-related protein that regulates microtubule dynamics during mitotic spindle assembly. Cell 84, 37–47.
Welte MA (2004). Bidirectional transport along microtubules. Curr Biol 14, R525–537.
Witczak O, Skalhegg BS, Keryer G, Bornens M, Tasken K, Jahnsen T, Orstavik S (1999). Cloning and characterization of a cDNA encoding an A-kinase anchoring protein located in the centrosome, AKAP450. EMBO J 18, 1858–1868.
Wittmann T, Waterman-Storer CM (2001). Cell motility: can Rho GTPases and microtubules point the way? J Cell Sci 114, 3795–3803.
Zaliapin I, Gabrielov A, Keilis-Borok V (2004). Multiscale trend analysis. Fractals 12, 275–292.
Zheng Y, Wong ML, Alberts B, Mitchison T (1998). Purification and assay of gamma tubulin ring complex. Methods Enzymol 298, 218–228.